ADVANCED MATERIALS INTERFACES

www.advmatinterfaces.de

Electronic Transport and Ferroelectric Switching in Ion-Bombarded, Defect-Engineered $BiFeO_3$ Thin Films

*Sahar Saremi, Ruijuan Xu, Liv R. Dedon, Ran Gao, Anirban Ghosh, Arvind Dasgupta, and Lane W. Martin**

Despite continued interest in the multiferroic $BiFeO_3$ for a diverse range of applications, use of this material is limited by its poor electrical leakage. This work demonstrates some of the most resistive $BiFeO_3$ thin films reported to date via defect engineering achieved via high-energy ion bombardment. High leakage in as-grown $BiFeO_3$ thin films is shown to be due to the presence of moderately shallow isolated trap states, which form during growth. Ion bombardment is shown to be an effective way to reduce this free carrier transport (by up to ≈4 orders of magnitude) by trapping the charge carriers in bombardment-induced, deep-lying defect complexes and clusters. The ion bombardment is also found to give rise to an increased resistance to switching as a result of an increase in defect concentration. This study demonstrates a systematic ion-dose-dependent increase in the coercivity, extension of the defect-related creep regime, increase in the pinning activation energy, decrease in the switching speed, and broadening of the field distribution of switching. Ultimately, the use of such defect-engineering routes to control materials will require identification of an optimum range of ion dosage to achieve maximum enhancement in resistivity with minimum impact on ferroelectric switching.

1. Introduction

Considerable effort in modern materials science has focused on the quest for multifunctional materials with novel or enhanced responses as a means to meet the needs of a diverse range of applications. Complex-oxide ferroelectric thin films have been extensively studied due to the existence of spontaneous switchable polarization and strong coupling between their electrical, mechanical, thermal, and optical responses.[1–23] Among complex-oxide ferroelectrics, $BiFeO_3$ has attracted considerable attention due to its multiferroic nature (i.e., coexistence of a large spontaneous polarization and G-type antiferromagnetism), and potential for strong magnetoelectric coupling.[4–6] Deterministic control of this material, however, is challenging due to the complex nature of its chemistry and penchant for defects (i.e., the presence of multiple cation and anion species and their corresponding point defects, complexes, and clusters). Similar to many other complex-oxide ferroelectrics, $BiFeO_3$ is known to be highly susceptible to point defect formation (which have low energy barriers of formation) and likely to create defects to maintain charge neutrality to compensate for impurities (often present in the source materials) and/or nonstoichiometry in the lattice.[7,8] The uncontrolled defect formation, in turn, can have a detrimental impact on the properties.[9] Therefore, careful understanding of the interplay between defects and materials response, as well as establishing routes to control the type and concentration of defects, are crucial for fine-tuning and optimization of the properties of $BiFeO_3$ thin films. For example, point defects often give rise to high leakage and losses via doping of the lattice with charge which can limit the application of $BiFeO_3$ thin films in electronic devices.[10–14] In turn, developing routes to enhance the resistivity of $BiFeO_3$ remains an important materials challenge. More broadly, defects can also have an impact on ferroelectric switching by controlling the local polarization stability, acting as pinning sites for domain-wall motion, and serving as nucleation sites for polarization reversal which can also place limitations on device-relevant parameters such as coercivity, energy of switching, switching speed, and more.[9,15] Although the prominent role of extended defects in ferroelectric switching is well understood,[16,17] there is less agreement on the effect of point defects. Some reports have suggested that point defects have a weak impact on domain-wall motion, while others have suggested more strong interactions.[18–21] Despite the known relevance of defects in ferroelectric switching, limited systematic studies have been undertaken on the interplay of defects and switching in $BiFeO_3$.

In order to reduce the electronic leakage in $BiFeO_3$, chemical doping/alloying (i.e., introduction of *extrinsic* defects/dopants)

S. Saremi, R. Xu, L. R. Dedon, R. Gao, Dr. A. Ghosh, A. Dasgupta, Prof. L. W. Martin
Department of Materials Science and Engineering
University of California
Berkeley, Berkeley, CA 94720, USA
E-mail: lwmartin@berkeley.edu
A. Dasgupta, Prof. L. W. Martin
Materials Sciences Division
Lawrence Berkeley National Laboratory
Berkeley, CA 94720, USA

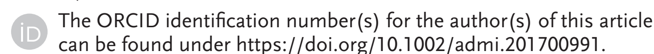
The ORCID identification number(s) for the author(s) of this article can be found under https://doi.org/10.1002/admi.201700991.

DOI: 10.1002/admi.201700991

© 2017 WILEY-VCH Verlag GmbH & Co. KGaA, Weinheim

has been traditionally used.[22–26] The extent to which the resistivity can be enhanced using chemical doping is, however, limited by the solid solubility, as well as by the simultaneous changes in the ferroelectric properties (e.g., reduction in polarization).[27] More broadly, in other systems such as group IV and III–V semiconductors, it has been shown that, in addition to *extrinsic* dopants, controlled introduction of *intrinsic* defects (i.e., vacancies, interstitials, and antisites related to the constituent elements, as well as their complexes and clusters) via ion bombardment can be an alternative and effective route to enhance resistivity. This technique enables the production of specific regions of high resistivity on a wafer due to the formation of mid-gap states, and isolation of neighboring active device regions (hence the name "ion bombardment for isolation").[28] In the case of complex oxides, prior work in this regard has been used in a similar sense—to locally disrupt or turn-off response,[29–31] but recent work in ferroelectrics has demonstrated that, when applied appropriately, such approaches can dramatically enhance the resistivity in $PbTiO_3$ thin films by controlling the concentration of *intrinsic* defects via high-energy ion bombardment thereby improving their ferroelectric performance.[32]

In this work, we address the leakage problem in $BiFeO_3$ thin films via high-energy ion bombardment. The ability of this ion-bombardment technique to control the concentration of *intrinsic* defects beyond the thermodynamic limits enables tuning of the resistivity by orders of magnitude, here demonstrated in some of the most resistive $BiFeO_3$ thin films reported to date. The defects responsible for the high leakage currents and lossy ferroelectric properties in as-grown $BiFeO_3$ thin films are identified to be isolated point defects such as oxygen vacancies, which dope the lattice with electrons and contribute to *n*-type conduction. Ion bombardment is shown to be an effective way to reduce the free carrier transport by trapping the charge carriers deep in the band gap as a result of the formation of bombardment-induced deep-lying defect complexes and clusters. This, in turn, gives rise to a dramatic reduction of leakage currents by up to ≈4 orders of magnitude and improvement of ferroelectric hysteresis response. Introduction of such defects, however, is also found to impact the switching behavior. Using a combination of piezoresponse force microscopy, macroscale capacitor-based switching kinetics, and first-order reversal curve (FORC) analysis it is shown that the increased defect concentrations, while having no evident impact on the domain structure or the switching mechanism, do give rise to a systematic increase in the coercivity, an extension of the defect-related creep regime, an increase in the pinning activation energy, a decrease in the switching speed, and a broadening of the field distribution of switching. Ultimately, such defect-engineering routes to enhance ferroelectric device performance require finding an optimum range of ion dosage to achieve maximum enhancement in resistivity with minimum impact on the ferroelectric switching.

2. Results and Discussion

100 nm $BiFeO_3$/20 nm $SrRuO_3$/$DyScO_3$ (110) thin-film heterostructures were grown via pulsed-laser deposition (Experimental Section). θ–2θ X-ray diffraction studies (Panalytical, X'pert[3] MRD) of as-grown heterostructures (**Figure 1**a,b, top) reveal that the heterostructures are epitaxial, 00*l*-oriented, and single-phase. Rutherford backscattering spectrometry (RBS) studies (Figure S1, Supporting Information) show that these growth conditions produce a nearly stoichiometric cation ratio ($Bi_{0.99}Fe_{1.00}O_x$), within the error of the RBS (±1–2%). These heterostructures were subsequently bombarded with varying dosages (10^{14}–10^{16} cm^{-2}) of He^{2+} ions with an energy of 3 MeV across the entire sample (Experimental Section). The high energy of the ions in these experiments allows for generation of *intrinsic* point defects without implantation in the ferroelectric as supported by stopping and range of ions in matter (SRIM) simulations (Experimental Section). The simulations suggest that the given experimental parameters will result in the He^{2+} ions being stopped deep within the $DyScO_3$ substrate (peaked around a depth of ≈15 µm), resulting in (effectively) zero concentration of He^{2+} ions throughout the thickness of the $BiFeO_3$ and $SrRuO_3$ layers (Figure S2a, Supporting Information). Further simulations show that Bi, Fe, and O vacancies are formed in the film, with a total defect concentration in the range of 10^{18}–10^{20} cm^{-3} for the dosage range of 10^{14}–10^{16} cm^{-2} (Figure S2b, Supporting Information), as a result of collision events between the high-energy He^{2+} ions and the target atoms. It should also be noted that the concentration of defects generated by the ion beam is relatively uniform throughout the thickness of the ferroelectric layer.

A signature of these ion-bombardment-induced defects can be found in the θ–2θ X-ray diffraction scans for the heterostructures bombarded with dosages of 10^{15} cm^{-2} (Figure 1a,b, middle) and 10^{16} cm^{-2} (Figure 1a,b, bottom). Although the films remain crystalline, epitaxial, and single-phase, there is a clear broadening of the film peak (suggesting a lowering of crystalline quality), and a slight out-of-plane lattice expansion which is attributed to the formation of point defects (indicated by a shift of the film peak to lower 2θ angles). The ion-dose-dependent reduction of the crystalline quality is further evidenced by a gradual increase in the full-width-at-half-maximum (FWHM) of the ω-scans (rocking curves) about the 002-diffraction conditions for the film and substrate (Figure 1c). The FWHM of the film peak changes from 0.045° for the as-grown heterostructures to 0.098° after bombardment with an He^{2+} dose of 10^{16} cm^{-2}. The FWHM for the substrate is shown for comparison (0.007°–0.011°). RBS studies were also completed after ion bombardment at a dosage of 10^{16} cm^{-2} (Figure S1, Supporting Information), and reveal no change in the overall chemistry of the heterostructures, suggesting that the bombardment-induced defects are produced in a stoichiometric fashion for all dosages studied herein.

In order to study the ion-dose-dependence of the properties, symmetric $SrRuO_3$ capacitor structures were fabricated using established techniques (Experimental Section).[33] The as-grown heterostructures show high leakage current density (Figure 1d, black data) and, as a result, the ferroelectric hysteresis loops are not fully saturated and closed (Figure 1e, black data). As mentioned earlier, this high leakage current is a common feature of $BiFeO_3$ and is the result of the presence of point defects which form during the growth as well as impurities in the target materials, which in turn dope the lattice with free charge and give rise to electronic conduction.[10–14] In turn, a systematic

© 2017 WILEY-VCH Verlag GmbH & Co. KGaA, Weinheim

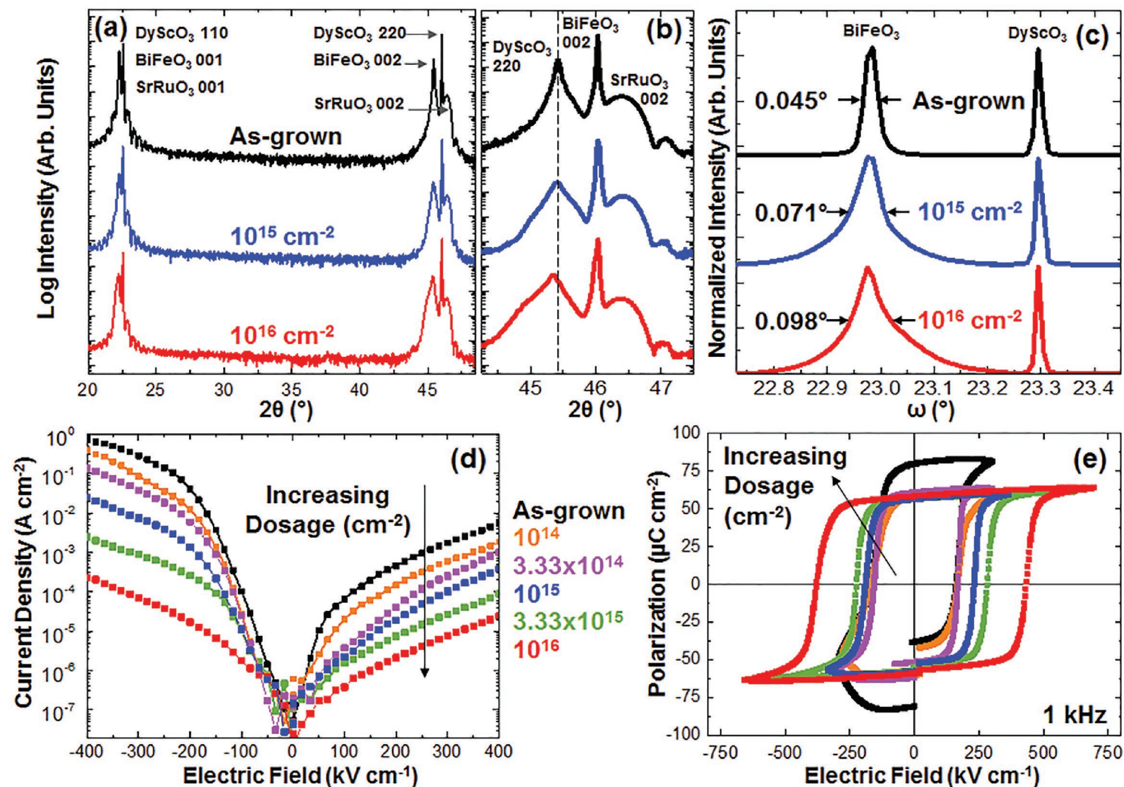

Figure 1. a) Wide-angle 2θ–ω X-ray diffraction scans and b) zoom-in about the 002- and 220-diffraction conditions for heterostructures ion bombarded with various He^{2+} dosages. c) Rocking curves for heterostructures ion bombarded with various He^{2+} dosages obtained about the 002-diffraction conditions of film and substrate. d) Leakage current density as a function of DC electric field, and e) ferroelectric polarization–electric field hysteresis loops measured at 1 kHz after ion bombardment with various He^{2+} dosages.

reduction in the leakage current density by up to ≈4 orders of magnitude can be achieved by increasing the ion-bombardment dosage (Figure 1d). As a result of this improved resistivity, there is a clear enhancement in the ferroelectric hysteresis response (Figure 1e). In the dosage range of 10^{15}–10^{16} cm^{-2}, fully saturated and closed loops with polarizations of ≈60 μC cm^{-2} are observed. At first glance, these observations may not be consistent with the prevailing thought that the high conductivity in $BiFeO_3$ originates from the presence of defects and thus increasing the concentration of *intrinsic* defects via ion bombardment should likely have a deleterious effect on properties; which is in contrast to our observations. To understand these nonintuitive results we have used a combination of impedance spectroscopy, deep-level transient spectroscopy (DLTS), and temperature-dependent current–voltage (*I*–*V*) measurements to explore the mechanisms responsible for the observed changes.

Various contributions to the overall resistive response of a material can be differentiated via impedance spectroscopy (Experimental Section). Nyquist impedance plots can contain several semicircles wherein each semicircle is characteristic of a single time constant.[34,35] Therefore, these studies could be particularly useful to gain information on whether the increase in the resistivity as a result of ion bombardment is induced by changes at the film–electrode interfaces or from the formation of surface layers (e.g., due to the possibility of defect accumulation at the interfaces). Impedance spectroscopy measurements were carried out on heterostructures exposed to various ion-bombardment dosages including as-grown (no bombardment), 10^{15} cm^{-2}, and 10^{16} cm^{-2} and show the presence of only one semicircle for all dosages (**Figure 2**a). A zoom-in of the semicircle for each ion-bombardment dosage is also provided (Figure S3, Supporting Information). This suggests that the transport for all heterostructures is dominated by the bulk of the film. The magnitude of the resistance can be extracted from the intercept of the semicircles on the real axis. While transport remains bulk mediated, a clear and systematic increase in the resistance of the films can be observed as an increase in the radius of the semicircles with increasing ion-bombardment dosage; this is in agreement with the dose-dependent reduction of the current density as a function of DC bias (Figure 1d). The film resistance is found to increase from 1.4×10^{10} Ω for the as-grown heterostructure, to 7.8×10^{10} and 9.4×10^{11} Ω for the same heterostructure bombarded with dosages of 10^{15} and 10^{16} cm^{-2}, respectively.

Having established that the transport remains bulk mediated, we applied both temperature-dependent current–voltage (*I*–*V*) and DLTS measurements (Experimental Section and Supporting Information) to understand the origin of the large differences in the conductivity. Temperature-dependent *I*–*V* studies were carried out on heterostructures bombarded with various He^{2+} ion dosages (including as-grown (no bombardment), 10^{15} cm^{-2}, and 10^{16} cm^{-2}) in order to determine the dominant conduction mechanism and trap states. A number of potential transport mechanisms were considered,

© 2017 WILEY-VCH Verlag GmbH & Co. KGaA, Weinheim

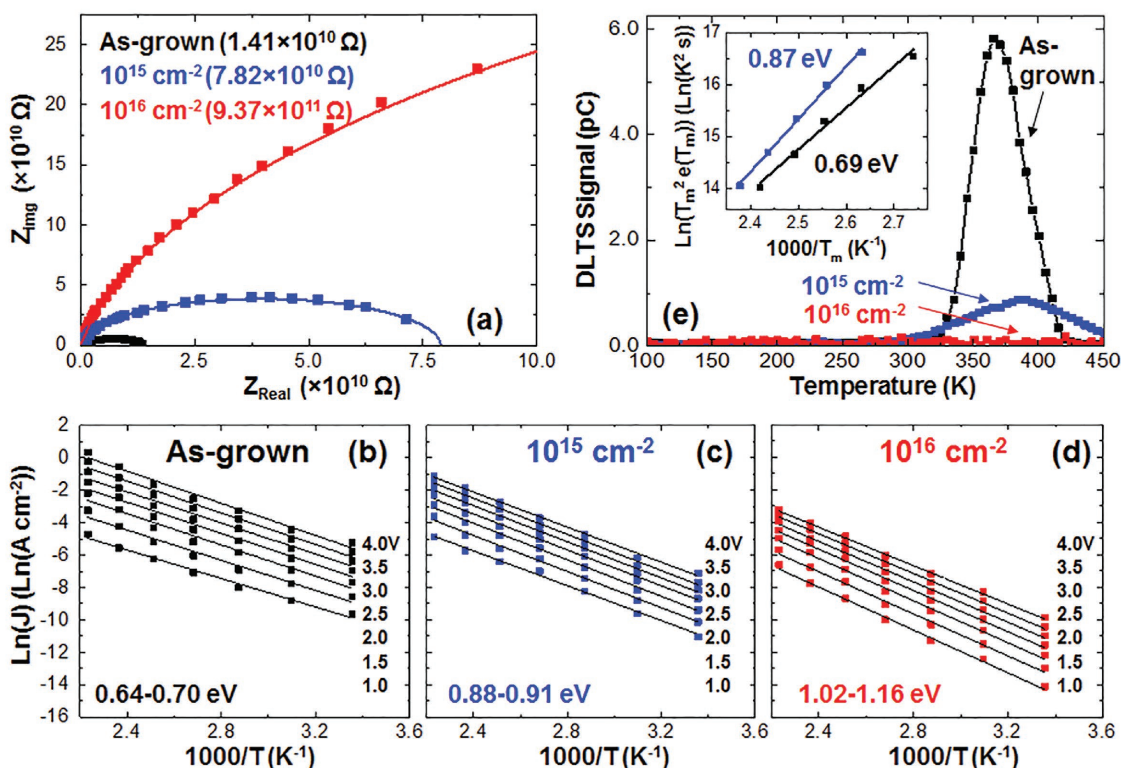

Figure 2. a) Nyquist plots (Z_{Img} vs Z_{Real}) for heterostructures ion bombarded with various He^{2+} dosages suggesting a single transport mechanism dominated by the bulk of the film with increasing resistance (extracted from the intercept of the semicircles on the real axis) with increasing dosage. Arrhenius plots of ln (J) versus $1000/T$ at different voltages for b) as-grown (no bombardment), c) 10^{15} cm^{-2}, and d) 10^{16} cm^{-2} heterostructures. The activation energies (noted) are extracted from the slope of the linear fits. Range of activation energies corresponds to small variation in the slope of the linear fits at different voltages. e) DLTS signal measured at the same rate window (80–160 ms) for heterostructures bombarded with various He^{2+} dosages. Inset shows the Arrhenius plot of $\ln\left(\frac{T_m^2}{e(T_m)}\right)$ versus $\frac{1000}{T_m}$, where T_m is the temperature at which the maximum of the DLTS peak occurs, obtained in a rate window between t_1 and t_2. $e(T_m)$ is the emission rate of a defect with DLTS peak located at T_m. The activation energy of each trap state (E_d) can be extracted from the slope of the linear fits.

and modified Poole–Frenkel emission was identified as the dominant mechanism for all heterostructures (Figure S4, Supporting Information). Poole–Frenkel emission is a bulk-limited conduction mechanism governed by field-assisted emission of carriers from internal trap states.[36] In situations where there are large concentrations of donor and/or acceptor states, the Poole–Frenkel emission model is modified by adding an exponential scaling term in order to fit the experimental data.[37,38] The $I–V$ response for all heterostructures was obtained at different temperatures (Figure S5, Supporting Information), and the activation energies were extracted from the slope of ln(J) versus $1000/T$ plots at different electric fields considering modified Poole–Frenkel emission (Figure 2b–d). While there is no change in the conduction mechanism, a systematic increase in the activation energy of the dominant trap states can be observed by increasing the ion-bombardment dosage wherein it increases from 0.64–0.70 eV for the as-grown heterostructures, to 0.88–0.91 and 1.02–1.16 eV for heterostructures ion bombarded with dosages of 10^{15} and 10^{16} cm^{-2}, respectively.

The main cause for high leakage currents in $BiFeO_3$ is known to be related to the presence of oxygen vacancies acting as donors, as well as to hopping of electrons from Fe^{2+} to Fe^{3+} which is expected in the presence of oxygen vacancies.[11,14,22,24–26] In turn, trap states in the range of 0.6–0.8 eV below the conduction band edge in $BiFeO_3$ have been attributed to such defects,[39] and are consistent with the activation energies extracted from our $I–V$ measurements for the as-grown heterostructures. These defects, in turn, dope the lattice with electrons and contribute to n-type conduction. The n-type nature of conduction in these as-grown $BiFeO_3$ films has been confirmed and reported elsewhere.[10] The higher activation energy of 1.02–1.16 eV extracted for the dominant trap state in highly ion-bombarded heterostructures (dosage of 10^{16} cm^{-2}), however, implies the formation of deeper trap states. These deep-lying, ion-bombardment-induced defects (which could be related to vacancies, interstitials, and/or antisites of any of the constituent elements and their complexes and clusters) can trap charge carriers deep in the band gap, and in turn, reduce the free carrier transport. Formation of damage-related deep levels upon ion bombardment is well known in semiconductors, and it has been shown that these induced mid-gap levels are responsible for trapping of free carriers and increasing the resistivity.[28]

In order to gain more insight on the type of ion-bombardment-induced defects, DLTS measurements were also carried out on the same heterostructures. DLTS is a technique capable

© 2017 WILEY-VCH Verlag GmbH & Co. KGaA, Weinheim

of probing multiple inter-gap trap states.[40] DLTS signals were obtained on heterostructures ion bombarded with various dosages (including as-grown (no bombardment), 10^{15} cm^{-2}, and 10^{16} cm^{-2}) in the temperature range 100–450 K for varying times t_1 and t_2 (i.e., different rate windows, in the range of 5–160 ms) (Figure S6, Supporting Information). For more clarity in comparing the results obtained at different dosages, only the DLTS signals obtained at one single rate window (80–160 ms) are shown (Figure 2e). A single DLTS peak is observed in the studied temperature range. The activation energies, extracted from the linear fits to the Arrhenius plots (Figure 2e, inset), are ≈0.69 eV for the as-grown heterostructures and ≈0.87 eV for the heterostructures ion bombarded to a dosage of 10^{15} cm^{-2}. No DLTS peak can be measured for the heterostructures ion bombarded to a dosage of 10^{16} cm^{-2} within the same temperature and rate windows. There is a close agreement between the activation energies extracted from DLTS and I–V measurements for the as-grown and 10^{15} cm^{-2} heterostructures, suggesting that the same trap states are probed by the two techniques. Furthermore, as the ion-bombardment dosage increases, the DLTS peak is found to decrease in intensity, broaden in shape, and shift to higher temperatures. Broadening of the shape and decreasing intensity of a DLTS peak are usually attributed to the formation of defect clusters which can give rise to a distribution in emission energies. Moreover, shifts of a peak can be caused by changes in the environment surrounding the defect or the defect configuration.[41,42] These observations indicate that the shallow trap state in the as-grown heterostructures is likely related to isolated point defects as suggested by the presence of a sharp and high intensity DLTS peak. As the concentration of defects increases as a result of ion bombardment, however, it is hypothesized that these isolated defects are transformed into defect complexes and clusters (composed of cation and/or anion vacancies, and potentially interstitials or antisites) which would be consistent with the lowering of the intensity, broadening, and shift of the DLTS peak. Therefore, it can be concluded that in addition to giving rise to the formation of deep-lying trap states, ion bombardment also results in an increased concentration of complex defects and clusters. Therefore, high-energy ion bombardment can be an effective technique for tuning the concentration and type of *intrinsic* defects, and in turn, tuning electrical properties and enhancing device performance, keeping in mind that the highly resistive state will be stable until it is exposed to temperatures at which the bombardment-induced defect states anneal out (Figure S7, Supporting Information). To better understand the potential of this technique for ferroelectric device performance optimization, however, the impact of these ion-bombardment-induced defects on the switching behavior should not be overlooked, due to the potentially prominent role of defects in ferroelectric switching.

In the following we focus on the study of polarization switching in ion-bombarded versions of $BiFeO_3$. Having the ability to tune the concentration of defects by means of ion bombardment allows for a systematic study of the effect of defects on the switching behavior in terms of mechanism, rate, and energy requirements. Examination of ferroelectric hysteresis loops (obtained at 10 kHz in order to minimize the effect of high leakage in the as-grown heterostructures) reveals a clear increase in the coercive field with increasing ion-bombardment dosage (**Figure 3**a). This increase in coercive field occurs even as no apparent change in the domain structure is detected by piezoresponse force microscopy (MFP-3D microscope, Asylum Research) upon ion bombardment even up to the maximum dosage of 10^{16} cm^{-2} (Figure S8, Supporting Information). A combination of macroscale switching kinetics and FORC studies are used to gain more insight into the origin of the dose-dependent changes of the coercivity.

In order to study the switching kinetics, pulsed measurements were used (Experimental Section) in which the change of polarization (ΔP) was probed as a function of voltage pulse width and amplitude (Figure S9, Supporting Information). The measurements were carried out on the heterostructures with various ion-bombardment dosages (as-grown (no bombardment), 10^{15} cm^{-2}, and 10^{16} cm^{-2}) (Figure S10, Supporting Information). The Kolmogorov–Avrami–Ishibashi model[43,44] was used to fit the experimental data (Supporting Information) and the switching speed, as a function of applied electric field at various dosages, was extracted from the fittings (Figure 3b). As predicted by classical models (Supporting Information), domain-wall velocity varies nonlinearly with electric field, and can be classified into creep (i.e., thermally activated, slow propagation of domain walls between pinning sites (e.g., local disorder such as defects)), depinning (i.e., transition from creep to flow), and flow (i.e., motion of domain walls free from pinning sites) regimes.[45]

For the heterostructures studied herein, the plot of switching speed versus electric field (Figure 3b) reveals that for all dosages, the domain-wall motion is in the creep regime. This is due to the fact that even in the as-grown heterostructure with no ion-bombardment, there is a nonzero concentration of defects (dictated by thermodynamics and growth) which can act as pinning sites. There is a systematic extension of the creep regime to higher electric fields, however, with increasing ion-bombardment dosage. This is consistent with defect-related creep motion in ferroelectrics. The pinning activation energy can be extracted from the fits to the plot of $\ln(\theta)$ versus $1/E$, where θ is the switching speed and E is the applied electric field (Figure 3b, inset). The linear nature of the fits suggests a long-range, random-field[45] pinning potential for all heterostructures (Supporting Information). The activation energies at room temperature are extracted from the slope of the linear fits, and show a systematic increase with increasing ion-bombardment dosage, from 1405 K MV cm^{-1} for the as-grown heterostructure, to 1598 and 3399 K MV cm^{-1} for the heterostructures ion bombarded with dosages of 10^{15} and 10^{16} cm^{-2}, respectively. Therefore, increasing the concentration of defects provides more pinning sites, increases the pinning activation energy, and increases the difficulty of domain-wall motion, which in turn gives rise to a dose-dependent increase of the coercive field.

Although switching kinetics studies provide valuable information about polarization switching dynamics at the macroscale, the switching process can vary locally due to the presence of disorder and randomness.[46] Therefore, macroscopic kinetics measurements and single major hysteresis loops measured between saturation fields are insufficient to fully describe the switching process. FORC measurements (which involve measurement of minor hysteresis loops and probe the polarization field dependence

© 2017 WILEY-VCH Verlag GmbH & Co. KGaA, Weinheim

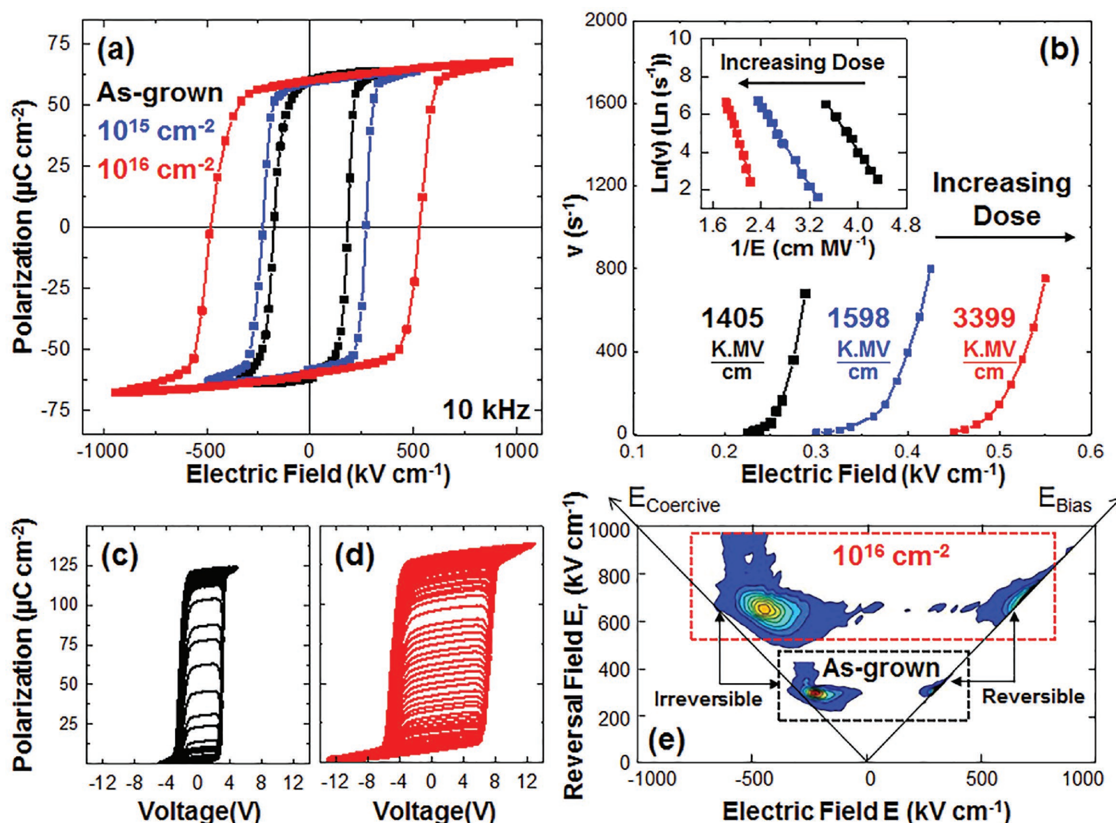

Figure 3. a) Ferroelectric polarization–electric field hysteresis loops measured at 10 kHz after ion bombardment with various He^{2+} dosages. b) Switching speed as a function of electric field for heterostructures ion bombarded with various He^{2+} dosages. Inset shows the plot of $\ln(V)$ versus $1/E$. The activation energies are extracted from the linear fits. The minor loops measured between the negative saturation field and various reversal fields (E_r) for c) as-grown (no bombardment) and d) 10^{16} cm^{-2} heterostructures. e) The FORC distributions for the as-grown (no bombardment) and 10^{16} cm^{-2} heterostructures.

between the saturation field and various reversal fields), on the other hand, can provide additional information on the characteristic microscopic mechanisms involved in switching.[47] FORC diagrams show a distribution of the elementary switchable units over their coercive and bias fields, in relation to the Preisach model.[47] In other words, they provide a map of the density of microscopic bistable polarizing units as a function of switching fields (i.e., a population/probability map of the switching fields), offering a graphical method to probe the (in)homogeneity of the switching events. In our particular case, such measurements can shine light on how the introduction of ion-bombardment-induced *intrinsic* defects and disorder change the switching process and its uniformity at the microscopic scale.

FORC measurements (Experimental Section) were carried out on the as-grown (no bombardment) and 10^{16} cm^{-2} ion-bombarded heterostructures (Figure 3c,d). The distribution functions are calculated (Supporting Information), and their contour plots are shown (Figure 3e). Note that, near the reversal field values, a measurable increase in polarization can be observed, even after the applied field starts to decrease (Figure 3c,d). In other words, there is a lag between the output (polarization) and the input (applied electric field). This effect can be attributed to the counterbalance between the applied electric field sweep rate and the switching time, and suggests a dynamic time-dependent hysteresis response, related to the kinetics of polarization switching. As discussed previously, the switching kinetics studies reveal that for all dosages studied herein, the domain-wall motion is in the creep regime (Figure 3b), which involves a thermally activated slow propagation of domain walls between pinning sites. As it can be seen, for all the dosages the characteristic switching speed is slower than the hysteresis period used for the measurement of the minor loops (10 kHz), as a result of which, the film continues to switch as the field is reduced after the reversal point. Although this lag between polarization and the applied field is less prominent for lower electric field sweep rates (not shown here), the data shown here was obtained at 10 kHz as the as-grown, unbombarded films are rather leaky at lower frequencies. Here we construct the FORC distributions using the classical Preisach model in order to qualitatively compare the effects of bombardment and defects on the distribution of the coercive fields of the elementary switchable units. We note, however, that if one desired to extract further quantitative information on the dynamics of the switching process from the FORC measurements, so-called dynamic/moving Preisach models of hysteresis which account for the time-dependent nature of the response via introduction of single or multiple relaxation times into the classical model would be required.[48]

© 2017 WILEY-VCH Verlag GmbH & Co. KGaA, Weinheim

Regardless, in this representation of the FORC data, the reversible (i.e., distribution along the bias axis) and irreversible contributions to the total polarization are observed to be separated (Figure 3e).[47] The overall shape of the distributions remains similar (i.e., in both cases, there is a larger distribution of coercive fields with a narrower distribution of bias fields) and the ratio of the reversible to irreversible contributions remains similar upon ion bombardment. The data suggest, however, that upon ion bombardment the polarization units become dispersed and distributed in a wider range of higher coercivities and bias fields. Ion bombardment clearly results in broadening and dispersion of the FORC distribution, and lowering of its maximum intensity. In the as-grown state, the distributions are, by comparison, narrower with a well-defined, high-intensity maximum, meaning that almost all the dipolar units are reversed in a limited range of fields. This suggests a reduction in the homogeneity of the ferroelectric switching upon ion bombardment, which is consistent with the fact that such high-energy ion bombardment results in an increase in the concentration of *intrinsic* point defects, formation of complexes and clusters, and hence an increase in the disorder of the system which results in less uniform switching. The maximum intensity corresponds to the most probable fields for the largest number of switchable units which make the largest contribution to the polarization switching. This intensity maximum shifts toward higher coercive and bias fields upon ion bombardment. The increase in the coercivity, as mentioned earlier, accounts for the pinning effect of defects on the domain walls. The bias-field distribution is indicative of the nanoscale imprint characteristics of the ferroelectric as it pertains to the preferential polarization of the switching units.[47] The combined knowledge gained from piezoresponse force microscopy, macroscale switching kinetics, and FORC studies suggest that the *intrinsic* defects formed during the ion bombardment do not have any effect on the domain structure or the switching mechanism, but do increase the disorder of the medium (broadening the field distribution for switching) that results in a systematic dose-dependent increase in the coercivity, extension of the defect-related creep regime, increase in the pinning activation energy, and decrease in the switching speed which altogether suggest an increased resistance to switching with increasing concentration of defects.

3. Conclusion

In conclusion, we have shown that high-energy ion bombardment can be a valuable technique for tuning the concentration and type of *intrinsic* defects in ferroelectric thin films and provides a route to a systematic study of defect–property relations. We have also demonstrated the potential of this ion bombardment for enhancement of the properties including multiple orders of magnitude enhancement in electrical resistivity, and in turn, improvement of ferroelectric hysteresis measurements, without suppression of the polarization values. Increasing the concentration of ion-bombardment-induced defects, however, can put a limit on ferroelectric device performance in that it strongly impacts switching properties due to the presence of strong defect–polarization coupling. Introduction of deep-lying ion-bombardment-induced defect complexes and clusters are shown to be responsible for a reduction of free carrier transport and hence the leakage current density, while on the other hand they give rise to an increased resistance to switching. Therefore, the application of this technique for enhancement of ferroelectric device performance requires finding an optimum range of ion dosage to achieve maximum enhancement in resistivity with minimum impact on the ferroelectric switching.

4. Experimental Section

Heterostructure Growth: Heterostructures were grown via pulsed-laser deposition using a KrF excimer laser (248 nm, Compex, Coherent), in an on-axis geometry. Films were grown on 20 nm $SrRuO_3/DyScO_3$ (110) single-crystal substrates (Crystec) from ceramic targets with chemistries $SrRuO_3$ and $Bi_{1.1}Fe_{1.0}O_3$. Targets were sanded, cleaned, and sufficiently preablated prior to every growth to assure the target surface had reached steady state prior to film deposition. The $SrRuO_3$ layer, to be used as a bottom electrode for subsequent electrical studies, was grown at a heater temperature of 700 °C in a dynamic oxygen pressure of 100 mTorr at a laser repetition rate of 15 Hz and a laser fluence of 1.3 J cm^{-2}. The $BiFeO_3$ films were grown at a heater temperature of 700 °C in a dynamic oxygen pressure of 100 mTorr at a laser repetition rate of 20 Hz, and a laser fluence of 1.1 J cm^{-2}. All substrates were adhered to the heater with Ag paint (Ted Pella, Inc.). Following growth, the heterostructures were cooled down to room temperature at a rate of 10 °C min^{-1}, in an oxygen pressure of 700 Torr.

Structure and Chemical Analysis: The structure of the heterostructures was probed using X-ray diffraction using a Panalytical X'Pert^3 MRD 4-circle diffractometer. Peak fitting to extract the FWHM values was done in the *X'Pert^3 Data Viewer* software. The chemistry of the ferroelectric layers was probed via RBS with an incident He-ion energy of 3040 keV, an incident angle $\alpha = 22.5°$, an exit angle $\beta = 25.35°$, and a scattering angle $\theta = 168°$ in the Cornell geometry. RBS samples were also grown on $DyScO_3$ (110) substrates simultaneously with the films studied herein. Fits to the experimental data were completed using the built-in fitting program in the RBS analysis software SIMNRA (simnra.com).

Ion Bombardment: Ion bombardment was carried out in the Pellatron located at Lawrence Berkeley National Laboratory using He^{2+} ions with an energy of 3 MeV and incident angle $\alpha = 0°$. A large aperture size (comparable to the size of the sample) was used in order to achieve a uniform irradiation dosage across the entire surface of the heterostructure.

SRIM Simulations: All simulations were made using SRIM 2013 (srim.org). SRIM is a group of programs which calculate the stopping and range of ions into matter using a quantum mechanical treatment of ion–atom collisions. Complex targets made of compound materials with up to eight layers can be defined, and final 3D distribution of the ions, target damage, sputtering, ionization, and phonon production can be simulated.

Top Electrode Growth: Top $SrRuO_3$ electrodes with a thickness of 80 nm were grown at 550 °C (in order to minimize bismuth-loss during processing) while all other conditions were the same as the bottom $SrRuO_3$. Top electrodes were patterned using MgO hard-mask in a circular shape with radius of 25 μm following established procedure.[33]

Transport and Ferroelectric Measurements: Transport and ferroelectric properties were measured using a Precision Multiferroic Tester (Radiant Technologies). Transport properties were measured in both positive and negative polarities, using an unswitched triangular voltage profile (in order to prevent any contributions from switching currents) with maximum ±4 V bias. Ferroelectric loops were obtained using a bipolar triangular voltage profile at frequencies in the range of 0.1–100 kHz. Switching pulsed measurements were completed using established voltage pulse sequences.[49] FORC measurements were carried out by measurement of multiple minor loops at 10 kHz using a monopolar

© 2017 WILEY-VCH Verlag GmbH & Co. KGaA, Weinheim

triangular voltage profile, between negative saturation field of each heterostructure and a variable reversal field (E_r), following the ascending branch of the major hysteresis loop. The FORC distributions were obtained from the mixed second derivative of polarization with respect to E and E_r.

Impedance Spectroscopy: Impedance spectroscopy is a powerful technique capable of differentiating between different contributions to the overall resistive response of a material. Impedance plots (imaginary vs. real) can contain several semicircles wherein each semicircle is characteristic of a single time constant or transport mechanism. Presence of multiple semicircles in the complex impedance plane can be attributed to bulk and grain-boundary responses, presence of mixed conduction (i.e., both electronic and ionic), contribution from surface layers, or sample–electrode interfaces. Impedance measurements were performed using Gamry Instruments-Reference 600 potentiostat, under an oscillation voltage of 8 mV_{rms}, in a frequency range of 10 mHz to 1 MHz.

DLTS: DLTS measurements were carried out using Precision Multiferroic Tester (Radiant Technologies), in a temperature range of 100–450 K with 5 K intervals, and 3 K min^{-1} ramp rate. The samples were kept for 5 min at each temperature before measurement. A +5 V pulse of 10 ms duration was applied to the samples, and the corresponding DLTS signal was measured at the end of the pulse using the conventional rate-window approach.[40] The DLTS signal (difference in transient capacitance at two different times t_1 and t_2 after the filling pulse) is then plotted as a function of temperature for five different rate windows ranging from 5 to 160 ms. Shifting of DLTS peaks can be obtained by varying the rate windows.

Supporting Information

Supporting Information is available from the Wiley Online Library or from the author.

Acknowledgements

S.S. acknowledges support from the National Science Foundation under grant CMMI-1434147. R.X. acknowledges support from the National Science Foundation under grant DMR-1708615. L.R.D. acknowledges support from the National Science Foundation under grant DMR-1608938. R.G. acknowledges support from the National Science Foundation under grant OISE-1545907. A.G. acknowledges support from the Gordon and Betty Moore Foundation's EPiQS Initiative, under grant GBMF5307. A.D. acknowledges support from the U.S. Department of Energy, Office of Science, Office of Basic Energy Sciences, under award number DE-SC-0012375 for development of ferroelectric thin films. L.W.M. acknowledges support from the Army Research Office under grant W911NF-14-1-0104.

Conflict of Interest

The authors declare no conflict of interest.

Keywords

bismuth ferrite, ferroelectric thin films, ion bombardment, leakage, polarization switching

Received: August 11, 2017
Revised: September 29, 2017
Published online:

[1] J. C. Agar, S. Pandya, R. Xu, A. K. Yadav, Z. Liu, T. Angsten, S. Saremi, M. Asta, R. Ramesh, L. W. Martin, *MRS Commun.* **2016**, *6*, 151.
[2] A. R. Damodaran, J. C. Agar, S. Pandya, Z. Chen, L. R. Dedon, R. Xu, B. Apgar, S. Saremi, L. W. Martin, *J. Phys.: Condens. Matter* **2016**, *28*, 263001.
[3] L. W. Martin, A. M. Rappe, *Nat. Rev. Mater.* **2016**, *2*, 16087.
[4] D. Sando, A. Barthelémy, M. Bibes, *J. Phys.: Condens. Matter* **2014**, *26*, 473201.
[5] L. W. Martin, D. G. Schlom, *Curr. Opin. Solid State Mater. Sci.* **2012**, *16*, 199.
[6] G. Catalan, J. F. Scott, *Adv. Mater.* **2009**, *21*, 2463.
[7] A. Lahmar, K. Zhao, S. Habouti, M. Dietze, C. H. Solterbeck, M. Es-Souni, *Solid State Ionics* **2011**, *202*, 1.
[8] M. Valant, A.-K. Axelsson, N. Alford, *Chem. Mater.* **2007**, *19*, 5431.
[9] D. Damjanovic, *Rep. Prog. Phys.* **1998**, *61*, 1267.
[10] L. R. Dedon, S. Saremi, Z. Chen, A. R. Damodaran, B. A. Apgar, R. Gao, L. W. Martin, *Chem. Mater.* **2016**, *28*, 5952.
[11] G. W. Pabst, L. W. Martin, Y.-H. Chu, R. Ramesh, *Appl. Phys. Lett.* **2007**, *90*, 072902.
[12] H. Yang, M. Jain, N. A. Suvorova, H. Zhou, H. M. Luo, D. M. Feldmann, P. C. Dowden, R. F. DePaula, S. R. Foltyn, Q. X. Jia, *Appl. Phys. Lett.* **2007**, *91*, 072911.
[13] C. Wang, M. Takahashi, H. Fujino, X. Zhao, E. Kume, T. Horiuchi, S. Sakai, *J. Appl. Phys.* **2006**, *99*, 054104.
[14] Y. P. Wang, L. Zhou, M. F. Zhang, X. Y. Chen, J.-M. Liu, Z. G. Liu, *Appl. Phys. Lett.* **2004**, *84*, 1731.
[15] S. M. Yang, J.-G. Yoon, T. W. Noh, *Curr. Appl. Phys.* **2011**, *11*, 1111.
[16] A. Y. Emelyanov, N. A. Pertsev, *Phys. Rev. B* **2003**, *68*, 214103.
[17] M. W. Chu, I. Szafraniak, D. Hesse, M. Alexe, U. Gosele, *Phys. Rev. B* **2005**, *72*, 174112.
[18] D. M. Marincel, *The Influence of Crystal Defects on Domain Wall Motion in Thin Film Pb(Zr,Ti)O_3*, The Pennsylvania State University, ProQuest Dissertations & Thesis Global, Ann Arbor, MI, USA **2014**.
[19] I. Fujii, M. Ugorek, Y. Han, S. Trolier-McKinstry, *J. Am. Ceram. Soc.* **2010**, *93*, 1081.
[20] D. Lee, B. C. Jeon, S. H. Baek, S. M. Yang, Y. J. Shin, T. H. Kim, Y. S. Kim, J.-G. Yoon, C. B. Eom, T. W. Noh, *Adv. Mater.* **2012**, *24*, 6490.
[21] Y. A. Genenko, J. Glaum, M. J. Hoffmann, K. Albe, *Mater. Sci. Eng., B* **2015**, *192*, 52.
[22] C.-H. Yang, D. Kan, I. Takeuchi, V. Nagarajand, J. Seidel, *Phys. Chem. Chem. Phys.* **2012**, *14*, 15953.
[23] Y.-H. Lee, J.-M. Wu, C.-H. Lai, *Appl. Phys. Lett.* **2006**, *88*, 042903.
[24] J. K. Kim, S. S. Kim, W.-J. Kim, A. S. Bhalla, R. Guo, *Appl. Phys. Lett.* **2006**, *88*, 132901.
[25] X. Qi, J. Dho, R. Tomov, M. G. Blamire, J. L. MacManus-Driscoll, *Appl. Phys. Lett.* **2005**, *86*, 062903.
[26] W. M. Zhu, Z.-G. Ye, *Ceram. Int.* **2004**, *30*, 1435.
[27] L. E. Cross, in *Ferroelectric Ceramics* (Eds: N. Setter, E. L. Colla), Birkhauser, Basel, Switzerland **1993**.
[28] S. J. Pearton, *Mater. Sci. Rep.* **1990**, *4*, 313.
[29] Y. Takamura, R. V. Chopdekar, A. Scholl, A. Doran, J. A. Liddle, B. Harteneck, Y. Suzuki, *Nano Lett.* **2006**, *6*, 1287.
[30] L. R. Zheng, P. X. Yang, L. W. Wang, C. L. Lin, S. C. Zou, *Nucl. Instrum. Methods Phys. Res., Sect. B* **1997**, *127*, 621.
[31] Y. Bastani, A. Y. Cortés-Peña, A. D. Wilson, S. Gerardin, M. Bagatin, A. Paccagnella, N. Bassiri-Gharb, *Appl. Phys. Lett.* **2013**, *102*, 192906.
[32] S. Saremi, R. Xu, L. R. Dedon, J. A. Mundy, S.-L. Hsu, Z. Chen, A. R. Damodaran, S. P. Chapman, J. T. Evans, L. W. Martin, *Adv. Mater.* **2016**, *28*, 10750.
[33] J. Karthik, A. R. Damodaran, L. W. Martin, *Adv. Mater.* **2012**, *24*, 1610.
[34] N. J. Donnelly, C. A. Randall, *Appl. Phys. Lett.* **2010**, *96*, 052906.

© 2017 WILEY-VCH Verlag GmbH & Co. KGaA, Weinheim

[35] A. R. West, D. C. Sinclair, N. Hirose, *J. Electroceram.* **1997**, *1*, 65.
[36] J. Frenkel, *Phys. Rev.* **1938**, *54*, 647.
[37] J. R. Yeargan, H. L. Taylor, *J. Appl. Phys.* **1968**, *39*, 5600.
[38] J. G. Simmons, *Phys. Rev.* **1967**, *155*, 657.
[39] S. J. Clark, J. Robertson, *Appl. Phys. Lett.* **2009**, *94*, 022902.
[40] D. V. Lang, *J. Appl. Phys.* **1974**, *45*, 3023.
[41] P. K. Giri, Y. N. Mohapatra, *Mater. Sci. Eng., B* **2000**, *71*, 327.
[42] M. Levinson, C. A. Aemiento, S. S. P. Shah, *MRS Online Proc. Libr.* **1987**, *92*, 353.
[43] M. Avrami, *J. Chem. Phys.* **1940**, *8*, 212.
[44] Y. Ishibash, Y. Takagi, *J. Phys. Soc. Jpn.* **1971**, *31*, 506.
[45] J. Y. Jo, S. M. Yang, T. H. Kim, H. N. Lee, J.-G. Yoon, S. Park, Y. Jo, M. H. Jung, T. W. Noh, *Phys. Rev. Lett.* **2009**, *102*, 045701.
[46] S. Zhukov, Y. A. Genenko, H. von Seggern, *J. Appl. Phys.* **2010**, *108*, 014106.
[47] A. Stancu, D. Ricinschi, L. Mitoseriu, P. Postolache, M. Okuyama, *Appl. Phys. Lett.* **2003**, *83*, 3767.
[48] I. D. Mayergoyz, *Mathematical Models of Hysteresis*, Springer, New York, NY, USA **1991**.
[49] A. K. Tagantsev, I. Stolichnov, N. Setter, *Phys. Rev. B* **2002**, *66*, 214109.

© 2017 WILEY-VCH Verlag GmbH & Co. KGaA, Weinheim